

# Strength and stiffness of cold-formed steel portal frame joints using quasi-static finite element analysis

Chia Mohammadjani, Amir M. Yousefi, Shu Qing Cai, G. Charles Clifton and James B.P. Lim\*

Department of Civil Engineering and Environmental Engineering, The University of Auckland, New Zealand

(Received May 31, 2017, Revised August 30, 2017, Accepted September 19, 2017)

**Abstract.** This paper describes a quasi-static finite element analysis, which uses the explicit integration method, of the apex joint of a cold-formed steel portal frame. Such cold-formed steel joints are semi-rigid as a result of bolt-hole elongation. Furthermore, the channel-sections that are being connected have a reduced moment capacity as a result of a bimoment. In the finite element model described, the bolt-holes and bolt shanks are all physically modelled, with contact defined between them. The force-displacement curves obtained from the quasi-static analysis are shown to be similar to those of the experimental test results, both in terms of stiffness as well as failure load. It is demonstrated that quasi-static finite element analysis can be used to predict the behavior of cold-formed steel portal frame joints and overcome convergence issues experienced in static finite element analysis.

**Keywords:** cold-formed steel; bolted moment-connections; finite element analysis; quasi-static

## 1. Introduction

The use of cold-formed steel as structural members is growing due to its fast construction speed as well as high strength-to-weight ratio (Kwon *et al.* 2014, Biggs *et al.* 2015, Zhou and Jiang 2017); for such members, the efficiency of connections between is important to improve the entire structural system (Qin and Chen 2016).

In regard to cold-formed steel portal frames (see Fig. 1), where the joints are moment-resisting, connections have an even more important role. Such frames are capable of spanning up to 30 m. Recent full-scale tests have been described by Zhang *et al.* (2015, 2016), primarily concerned with overall frame behaviour under lateral load. The joints used knee braces to sustain the bending moment at the eaves, as opposed to bolted moment connections.

For cold-formed steel portal frames that use bolted moment connections (see Fig. 2), the eaves and apex joints are of finite connection-length, semi-rigid and the joints (or more specifically the channel-sections being connected through the joints) have a reduced strength as a result of a bimoment caused by moment transfer being through bolt-holes in the webs Lim *et al.* (2016). Four full-scale apex joint tests have been described by Lim and Nethercot (2003) that specifically investigate this bimoment mode of failure of the channel-sections i.e., in these tests sufficient lateral restraint was provided to the joints to prevent overall buckling and in-plane failure of the channel-sections occurred owing to the bimoment, without any out-of-plane failure of the apex brackets. A photograph of the apex joint laboratory test by Lim and Nethercot (2003) is shown in



Fig. 1 Photograph of cold-formed steel portal frame after Wrzesien *et al.* (2015)

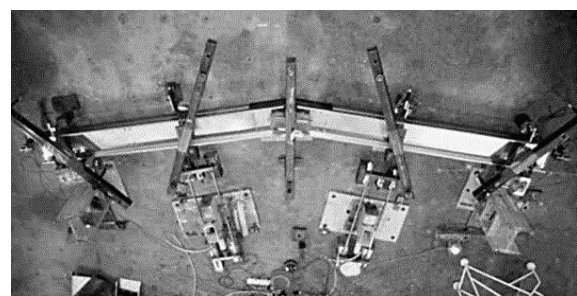


Fig. 2 Photograph of laboratory test set-up of apex joint after Lim and Nethercot (2003)

Fig. 2. More recently, Öztürk and Pu (2015) have also described laboratory apex joint tests, but these tests were not specifically detailed to investigate only bimoment failure, with failure occurring through buckling of the apex bracket.

In terms of overall frame behaviour, joints having a higher rotational stiffness and higher strength are clearly desirable, since frame design is often controlled by serviceability requirements (Phan *et al.* 2013). However,

\*Corresponding author, Associate Professor  
E-mail: [james.lim@auckland.ac.nz](mailto:james.lim@auckland.ac.nz)

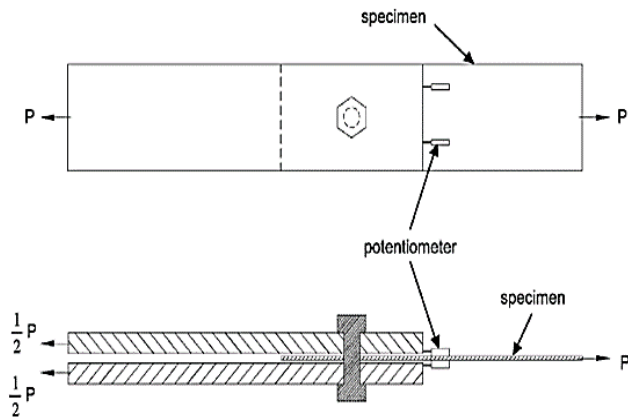


Fig. 3 Laboratory test set-up to measure bolt-hole elongation after Lim and Nethercot (2003)

this requires larger bracket sizes which would become more difficult to handle on site.

This paper is concerned with non-linear elasto-plastic quasi-static finite element models of the full-scale apex joints of Lim and Nethercot (2003), used to investigate the bimoment mode of failure, with the objective of being able to capture both the strength and stiffness of the bolted-moment connections, with the stiffness attributed to bolt-hole elongation. The finite element models described use similar modelling techniques described recently by Natário *et al.* (2014a, b) and Yousefi *et al.* (2017a, b) for web crippling, and also Öztürk and Pu (2015). The models use solid elements for modelling the cold-formed steel around the bolt-holes, thus allowing bolt-hole elongation to be captured through the contact between the bolt-holes and the bolt-shank. Solution parameters are investigated to see how they affect the accuracy of the results. While it should be emphasised that the Authors imply no novelty in terms of the modelling techniques employed, use of non-linear elasto-plastic static analysis with the same model resulted in non-convergence.

The results of the quasi-static models show good agreement against the experimental test results reported by Lim and Nethercot (2003), and demonstrate that the framework presented by Natário *et al.* (2014a, b) for web crippling can be successfully extended to other problems in cold-formed steel.

## 2. Experimental study

### 2.1 Lap joint tests in double shear

Details of the test specimen used to measure bolt-hole elongation are shown in Fig. 3. The plate was of nominal thickness 3 mm, width 100 mm and length 340 mm. The end distance measured from the centre of the bolt-hole to the edge of the plate was 80 mm. The bolt-hole elongation is given by the displacement of the LVDTs shown. The nominal diameter of the bolt-shank and bolt-hole were again 16 mm and 18 mm, respectively. The average yield and ultimate strengths of the plate, measured from three tensile coupons, were  $343 \text{ N/mm}^2$  and  $431 \text{ N/mm}^2$ ,

Table 1 Dimension of apex brackets tested by Lim and Nethercot (2003)

Joint test	Bracket			Bolt-group	
	$a$ (mm)	$b$ (mm)	$t$ (mm)	$a_B$ (mm)	$b_B$ (mm)
A	525	340	3.98	315	230
B	600	340	3.98	390	230
C	675	340	3.98	465	230
D	825	340	3.98	615	230

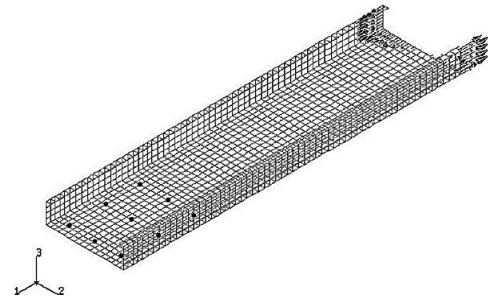


Fig. 4 Details of shell finite element idealization after Lim and Nethercot (2003)

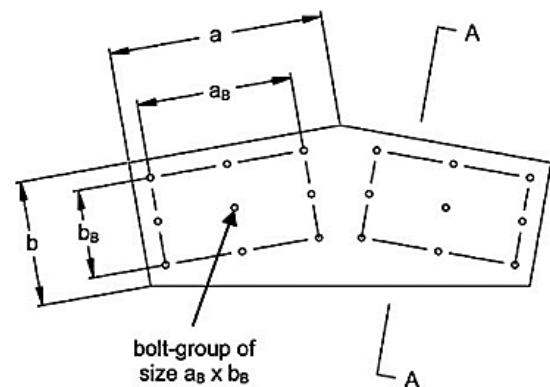


Fig. 5 Diagram showing parameters of apex bracket after Lim and Nethercot (2003)

respectively. It should be noted that the plate used for these tests was not the same as that used for either the apex bracket or channel-section in the apex joint tests to be described in the next Section.

As can be seen from Fig. 3, the plate was tested in a double-shear bolted lap-joint arrangement. The thickness of the two outer plates of mild steel was 15.8 mm. As this is approximately five times that of the plate under consideration, any elongation of the bolt-holes in the outer plates may be ignored. The bolt was finger-tightened. The double-shear bolted lap-joint test was conducted in a tensile testing machine and the elongation of the bolt-hole was measured using four potentiometers as shown. The extension rate used was 1 mm per minute and data was recorded at the rate of 10 readings per second.

### 2.2 Apex joint tests

Four apex joints were tested by Lim and Nethercot (2003). The parameters used to define the geometry of the

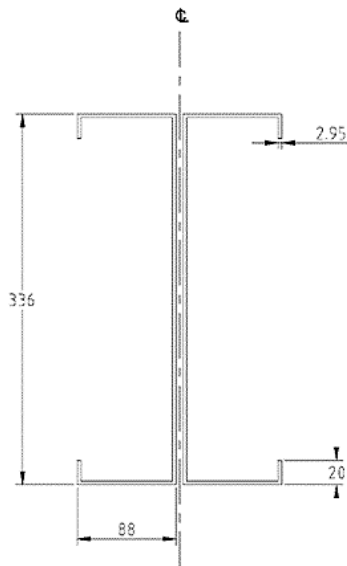


Fig. 6 Dimensions of back-to-back channel-sections

Table 2 Experimental and finite element results

Joint test	$a_B$ (mm)	$a_B/D$	$M_u^{exp}$ (kN.m)	$M_u^{ana}$ (kN.m)	$M_u^{exp} / M_u^{ana}$
A	315	0.94	75.0	74.0	1.01
B	390	1.16	77.5	76.0	1.02
C	465	1.38	82.5	79.5	1.04
D	615	1.83	87.5	83.0	1.05

back-to-back apex brackets used in each test are shown in Fig. 5. The lip stiffener along the compression edge of the apex brackets prevents buckling of the free-edge. In all four tests, no buckling of the apex brackets was observed.

The dimensions of the apex bracket used for each joint are summarized in Table 1. Each joint used a different length of bolt-group (and therefore a different size of apex bracket); all bolt-groups were formed from an array of nine bolts. The nominal thickness of each bracket was 4 mm and the nominal diameters of the bolts and bolt-holes were 16 mm and 18 mm, respectively. The average yield and ultimate strengths of the brackets, measured from three tensile coupons taken from each bracket, were 341 N/mm<sup>2</sup> and 511 N/mm<sup>2</sup>, respectively. The average dimensions of the channel-sections used in the tests are shown in Fig. 6. The average yield and ultimate strengths of the channel-sections were 358 N/mm<sup>2</sup> and 425 N/mm<sup>2</sup>, respectively.

As can be seen from Fig. 2, the apex joint was tested horizontally on the laboratory floor. The apex joint was loaded under pure bending. Table 2 shows the ratio  $a_B/D$  and the ultimate moment  $M_u^{exp}$  for all four apex joints, where  $D$  is the overall depth of the channel-section.

For reference, the moment capacity of the back-to-back channel-sections was calculated to be 96.8 kNm. It can be seen from Table 2 that as the value of  $a_B/D$  increases, the ultimate moment also increases. For example, Joint A, having a ratio of  $a_B/D$  of 0.93, failed at a bending moment 23% less than the moment capacity of the back-to-back channel-section according to BS5950: Part 5 (1998). On the other hand, Joint D, having a ratio of  $a_B/D$  of 1.81, failed at

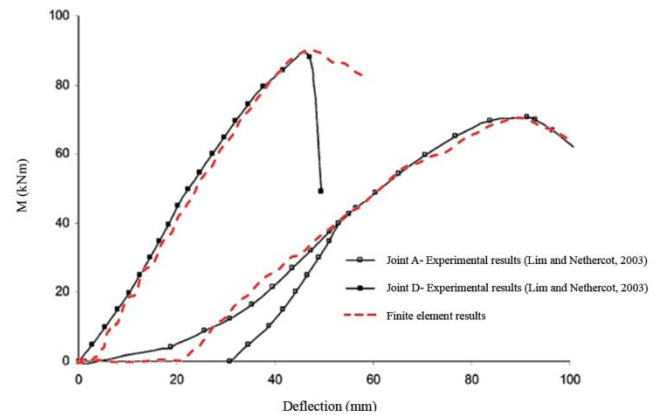


Fig. 7 Variation of load against deflection of Joints A and D after Lim and Nethercot (2003)

a bending moment only 10% less than the moment capacity of the back-to-back channel-sections.

Fig. 7 shows the variation of moment against apex deflection for Joints A and D. For the case of Joint A, it can be seen that the gradient of the load-deflection curve continues to increase until the load applied is approximately 5 kN. This gradual increase in the gradient of the load-deflection curve can be explained by the lack of perfect alignment of the bolt-holes in the channel-sections and brackets. For the case of the Joint D, the lack of alignment is not as noticeable. The sudden loss of load for Joint A at a bending moment of 40 kNm was due to slack in the loading rods not being removed. Inspection of the joint revealed no noticeable buckling of the channel-sections and so the joint was reloaded.

### 3. Analysis of bolt-hole elongation

A quasi-static model of the lap joint tests in double shear is described in this Section. The quasi-static model is analysed using explicit integration, using similar modelling techniques to those described for web crippling by Natário *et al.* (2014a, b). Natário *et al.* (2014a, b) presented that two methods can be used to reduce the computational time. The first method is to increase the rate at which the loading is applied. The second method is to use the mass scaling option and increase the density of all the elements in the model by a scaling factor. The second method is adopted in this paper. It should be noted that Section 4 will describe a quasi-static model of the apex joint tests. The finite element idealization described in this Section will be used for all bolt-holes in the apex joint model.

#### 3.1 Details of finite element model

Fig. 8 shows details of the laboratory test set-up to measure bolt-hole elongation after Lim and Nethercot (2003). Fig. 9 shows details of the finite element idealization of the lap joint in double shear. As can be seen from Fig. 9(c), since the lap joint is in double shear, only one plate has been modelled. While the plate is modelled using shell elements, an area 50 mm×50 mm around the

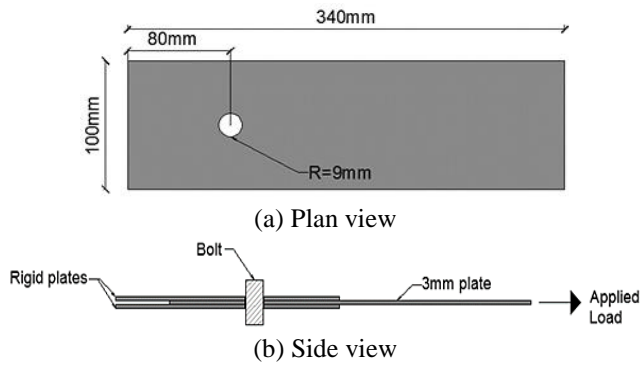


Fig. 8 Details of laboratory test set-up to measure bolt-hole elongation after Lim and Nethercot (2003)

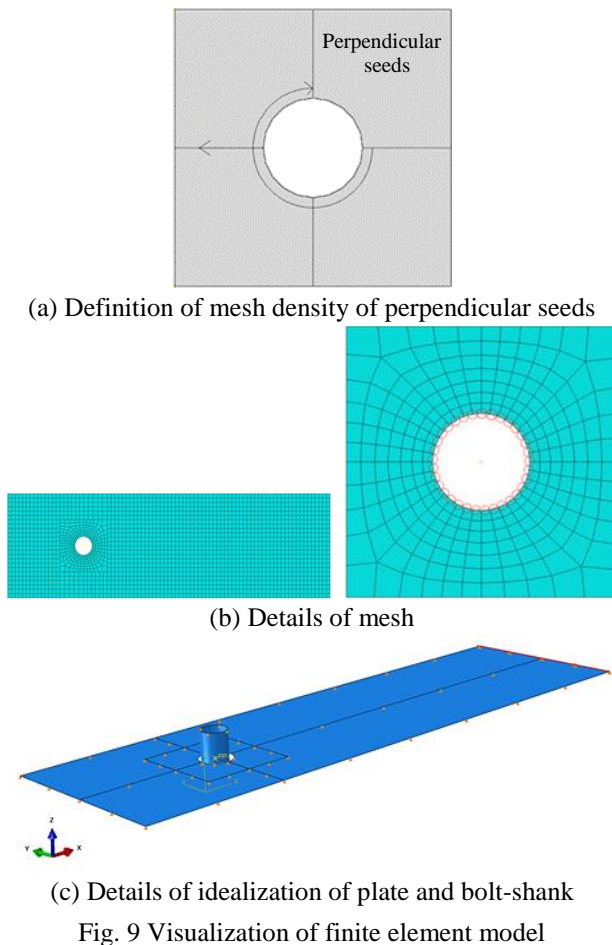


Fig. 9 Visualization of finite element model

bolt-hole of the plate is modelled using solid elements (C3D8R). The mesh was discretized such that it matched along the boundary between the solid elements and the shell elements.

For the solid elements, the mesh is labelled so that the mesh discretization can be identified from the label. For example, the label 40-7-2 means that there are 40 solid elements around the bolt hole, seven solid elements perpendicular to the bolt hole, and two solid elements through the thickness. As mentioned previously, the elements along the shell boundary edges was chosen to match.

As can also be seen from Fig. 9(c), the bolt is idealized

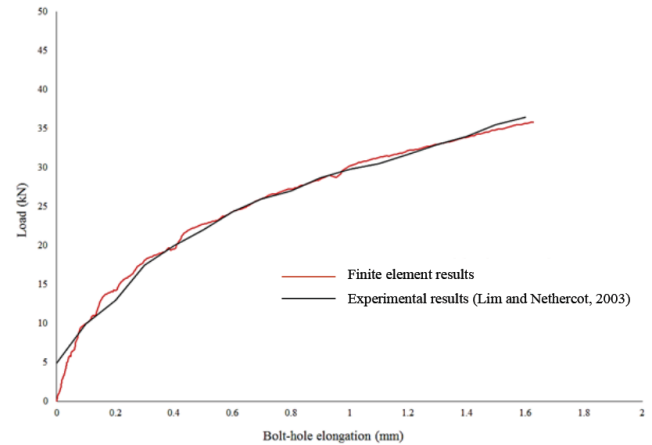


Fig. 10 Variation of force against bolt-hole elongation for model having mesh density of 40-7-2 and mass scaling of 100

as a hollow tube having a diameter of 16 mm and a length of 30 mm. The tube is essentially a rigid section, with all degrees of freedom restrained relative to a reference point, using the rigid body constraint option in the ABAQUS (2014) interaction module. For the analysis, a mass scaling factor of 100 was adopted; see section 4.3 for details.

Sabbagh *et al.* (2013), used a rigid plastic Cartesian element to consider the slip phenomenon inside the bolts. A similar method was followed in this paper with the difference of instead of assigning connector elements, the entire bolts were modelled in 3D.

### 3.2 Bolt-hole elongation results

Fig. 10 shows the variation of force against bolt-hole elongation using a mesh discretization of 40-7-2. Superimposed on Fig. 10 are the experimental test results. As can be seen, there is good agreement between the experimental test results and the finite element results.

A parametric study was then conducted on the mesh discretization of solid elements around the bolt hole. The process was similar to the job done by Liu *et al.* (2015) which determined the discretization pattern of the elements through the extensive trial and improvement process. Fig. 11 shows the variation of force against bolt-hole elongation for four different mesh discretization: 40-7-2, 40-7-2, 40-7-2, and 40-7-2.

From Fig. 11 it can be seen that the variation of load against bolt-hole elongation does not change for mesh discretization finer than that of 40-7-2. Fig. 12 shows the computational time required for each of the different mesh discretization. It can be seen that the model having a mesh discretization of 40-7-2 model required 70% of the computation time compared to that of the model having a mesh discretization of 48-7-2. Although the model having the 32-6-2 mesh discretization had a faster computational time than the model having the 40-7-2 mesh discretization, the initial stiffness was over-predicted. For the modelling of the bolt-holes of the apex joint described in Section 4, a model having a mesh discretization of 40-7-2 was therefore adopted.

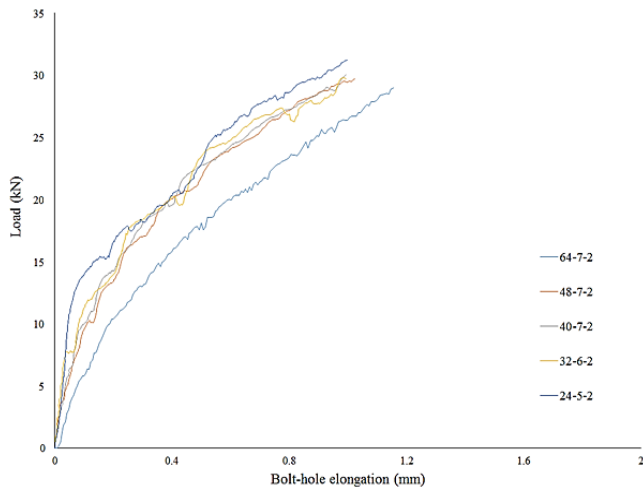


Fig. 11 Variation of force against bolt-hole elongation for different mesh densities and mass scaling of 100

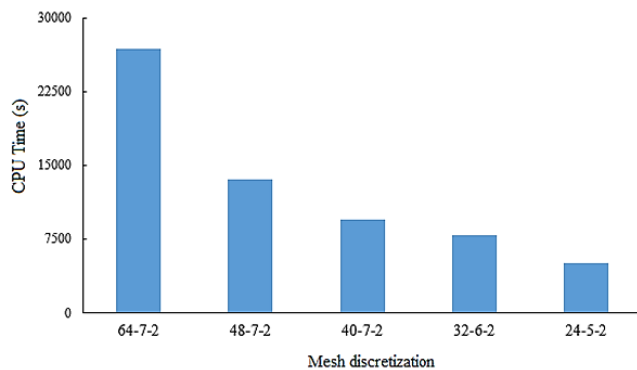


Fig. 12 CPU time for different models

## 4. Analysis of apex joint

### 4.1 Details of finite element model

On the day of the beam test, the respective control cylinders were capped and tested in compression to determine the compressive strength of concrete. Table 1 shows that the average values of the 56-day compressive strengths are 69.2 and 68.7 MPa for Series V and S specimens, respectively. The results indicate that although the two mix designs were different, they had similar compressive strength. Fig. 13 shows details of the experimental test setup. Fig. 14 shows details of the finite element idealization of the apex joint. As can be seen, quarter symmetry has been used with only one channel-section and one half of an apex joint modelled.

For symmetry, the apex bracket was prevented from translating along the centreline of the apex plate. Longitudinal movement of the roller was not prevented. Instead the web was prevented from moving out of plane 50 mm either side of the roller support. An area of 100 mm × 200 mm was prevented from moving in the out-of-plane direction around the loading pin.

Load was applied through a rigid body displacement of the bolt used for the jack, which was also restrained from moving in any other direction besides the loading direction.

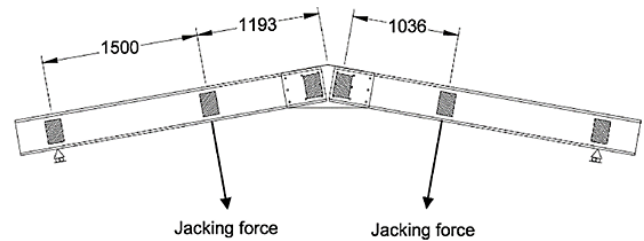


Fig. 13 Details of lateral restraint and loading applied to apex joint after Lim and Nethercot (2003)

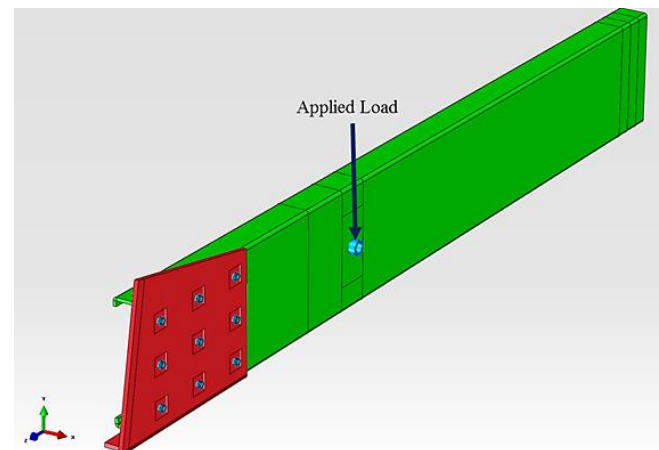


Fig. 14 Details of apex joint, bolts configuration and pin used to apply jacking force

Note: One half only shown with symmetry used at apex gusset plate centreline

All contacts in the assembly were modelled using the general contacts option.

### 4.2 Loading

To simulate the jacking force in the experimental set-up, a hole of 20 mm radius was modelled in the centre of the web and loaded through a rigid loading pin. The loading pin was displaced by 80 mm. The amount of displacement of the loading pin was controlled such that the velocity of the loading pin was slow enough to not significantly increase the kinetic energy of the model. As Bagheri Sabbagh *et al.* (2012), indicate in their research, a pretension force was applied to the bolts at the beam to the plate connection with the approximation of the 42% of the tensile strength of the bolts.

### 4.3 Mass scaling

Similar to the bolt-hole elongation model, the speed of analysis is highly dependent on the stable time increment of the models. However, the apex joint has a higher mass, compared with the bolt-hole elongation model, and also is longer in length, resulting in larger vibrational motion and therefore a higher kinetic energy.

The stable time increment is controlled by the solid elements around using to idealize the vicinity of the model around the bolt-holes. For the bolt-hole elongation model, a simple mass scaling factor of 100 was applied to the whole

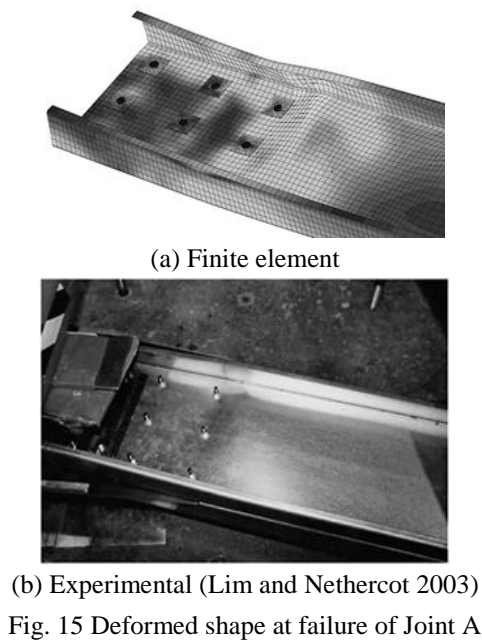


Fig. 15 Deformed shape at failure of Joint A

model and was sufficient to reduce the computation time to a reasonable level. Due to the small size of the model, the kinetic energy did not increase to significant amounts. In the apex joint model, however, such a mass scaling would cause kinetic energy to be unacceptable and so local mass scaling was adopted.

The mesh verification tool was used to detect and select the elements which limited the stable step sizes of the overall model. Three categories of mesh fineness were arbitrarily created and each were given their own levels of mass scaling. The first group were the elements which had a stable time increment of less than  $4 \times 10^{-6}$  seconds. The second set of elements were those whose stable time increment were greater than  $4 \times 10^{-6}$  seconds but less than  $4 \times 10^{-8}$  seconds. The final group of elements were those whose stable time increments were greater than  $8 \times 10^{-6}$  seconds but less than  $15 \times 10^{-6}$  seconds.

The first group of elements were given a mass scaling factor of 300. Although this is a high value of mass scaling, only the elements in the immediate vicinity of the bolt-holes were affected. Therefore, there was only a small increase in the total mass of the overall model. The second group of elements had a mass scaling factor of 100 and the third group a mass scaling factor of 80. The remaining element in the model had a mass scaling factor of 30. These values were selected such that the stable time increment after mass scaling of the smaller elements was not controlled by the stable time increment of the larger elements, which had a lower mass scaling factor.

#### 4.4 Apex joint analysis results

Fig. 7 also shows the variation of bending moment against displacement obtained from the finite element model of the apex joints. It should be noted that the finite element results have been *offset along the x-axis* so as to allow the load-displacement curves to be compared directly; the larger initial displacements in the experimental tests

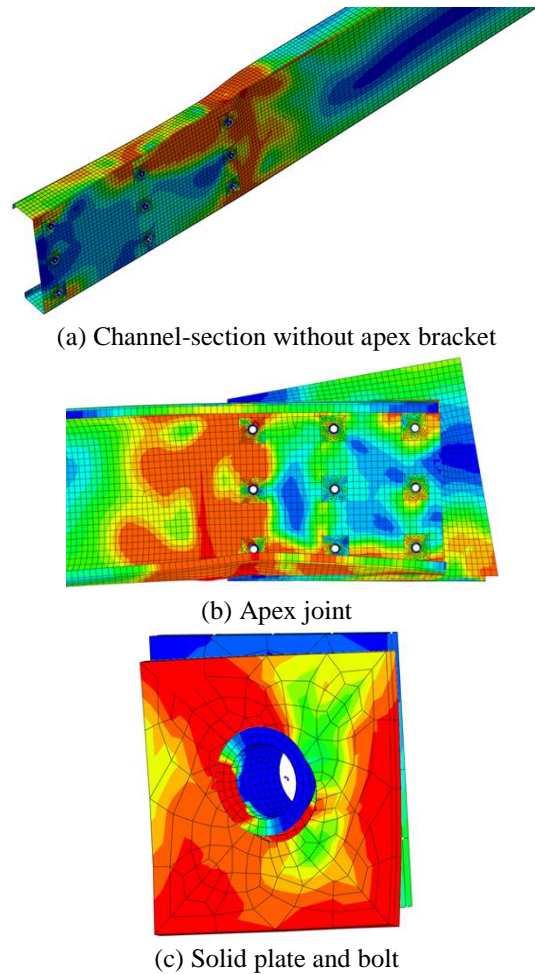


Fig. 16 Deformed shape of apex joint

results can be attributed to bolt-hole misalignment i.e. the gradual increase in the gradient may be explained by the lack of perfect alignment of the bolt holes due to human error during the drilling process; as a result, not all of the bolt shanks are in bearing contact against the bolt holes at the beginning of the test. As can be seen, the load-displacement curves of both Joints A and D are close those of the experimental tests.

Figs. 15 and 16 shows the deformed shape of Joint A at failure; the failure mode shape is also similar to that of the experimental test. In the finite element models it was noted that only that the bolts furthest away from the centre of the bolt-group were initially engaged. For example, for Joint D, the bolts nearer to the centre of the bolt-group were not engaged until the load applied was over 50 % of the failure load.

Table 2 summaries the failure loads predicted by the finite element analysis for the four different joint sizes. The failure loads recorded from the experimental tests are also shown. As can be seen, the failure loads predicted by the finite element model are slightly conservative to the experimental test results.

It should be noted that in the web-crippling model described by Natário *et al.* (2014a, b), the loading point was directly above the support point. On the other hand, for the model described in this paper, the loading point was located

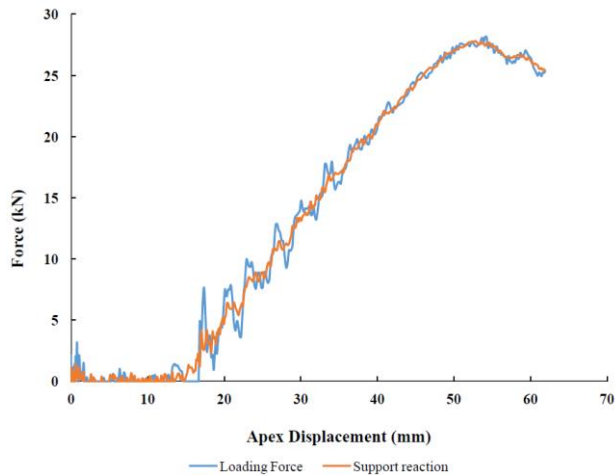


Fig. 17 Comparison of loading force and support reaction for Joint A

located 1.5 m away from the support point; the model can therefore be expected to be more susceptible to oscillating motions. To investigate this, Fig. 17 compares the loading force and support reaction for Joint A. Additionally, the variation of moment against displacement obtained numerically is shown in Fig.18 for all four joints described in Table 1 other joints. It should be noted that the results shown in Fig. 17 use the ABAQUS (2014) built-in graph smoothing function. The peak loads of the loading force and support reaction were 27 kN and 27.5 kN, respectively. The noise shown in Fig. 17 is typical of explicit dynamic analysis. In all models, the kinetic energy was below 5% of the total internal energy.

## 5. Conclusions

Natário *et al.* (2014a, b) has previously described the use of a quasi-static finite element analysis that used the explicit integration method, to predict the failure of cold-formed steel sections. This paper has adopted and extended the same quasi-static modelling approach to investigate the behavior of the apex joint of a cold-formed steel portal frame. Unlike the web crippling model of Natário *et al.* (2014a, b) where bolt-holes and bolt shanks were not required to be idealized, the apex joint model requires both in order to capture joint flexibility as well as failure of the channel-sections, as a result of load being transferred through the web generating a bimoment. Good agreement between previously reported experimental test results and the results obtained using the quasi-static analysis was shown. Using the modelling techniques described, quasi-static finite element analysis can therefore be used to predict the behavior of the joints of cold-formed steel portal frames, both in terms of strength as well as stiffness.

## Acknowledgments

The Ian and Emma Murry Trust and Auckland Doctoral Scholarship are gratefully thanked.

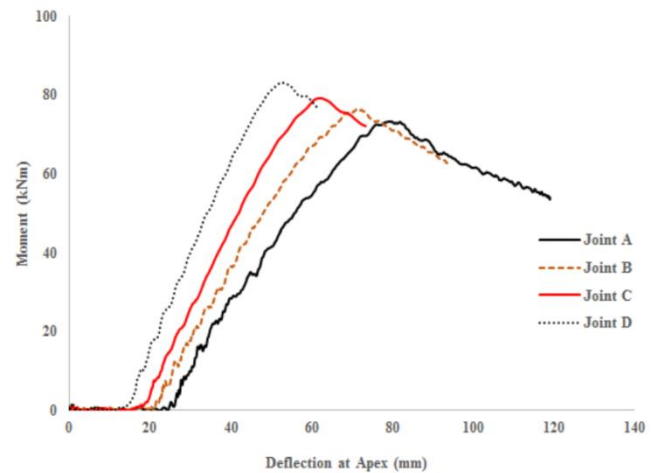


Fig.18 Variation of load against deflection for all joints in Table 1

## References

- ABAQUS (2014), Analysis User's Manual-Version 6.14-2 ABAQUS Inc., USA.
- Biggs, K.A., Ramseyer, C., Ree, S., and Kang, T.H.K. (2015), "Experimental testing of cold-formed built-up members in pure compression", *Steel Compos. Struct.*, **18**(6), 1331-1351.
- BS5950: Part 5 (1998), Code of practice for design of cold-formed sections, London, British Standards Institution.
- Kwon, Y.B., Kim, G.D. and Kwon, I.K. (2014), "Compression tests of cold-formed channel sections with perforations in the web", *Steel Compos. Struct.*, **16**(6), 657-679.
- Lim, J.B.P. and Nethercot, D.A. (2003), "Ultimate strength of bolted moment connections between cold-formed steel members", *Thin Wall. Struct.*, **41**(11), 10-19.
- Lim, J.B.P., Hancock, G.J., Clifton, G.C, Pham, C.H. and Das, R. (2016), "DSM for ultimate strength of bolted moment-connections between cold-formed steel channel members", *J. Constr. Steel Res.*, **117**, 196-203.
- Liu, Q., Yang, J. and Wang, F. (2015), "Numerical simulation of sleeve connections for cold formed steel sigma sections", *Eng. Struct.*, **100**, 686-695.
- Natário, P., Silvestre, N. and Camotim, D. (2014a), "Web crippling failure using quasi-static FE models", *Thin Wall. Struct.*, **84**, 34-49.
- Natário, P., Silvestre, N. and Camotim, D. (2014b), "Computational modelling of flange crushing in cold-formed steel section", *Thin Wall. Struct.*, **84**, 393-405.
- Oztürk, F. and Pul, S. (2015), "Experimental and numerical study on a full scale apex connection of cold-formed steel portal frames", *Thin Wall. Struct.*, **94**, 79-88.
- Phan, D.T., Lim, J.B.P., Tanyimboh, T.T., Lawson, R.M., Xu, Y., Martin, S. and Sha, W. (2013), "Effect of serviceability limits on optimal design of steel portal frames", *J. Constr. Steel Res.*, **86**, 74-84.
- Qin, Y. and Chen, Z. (2016), "Research on cold-formed steel connections: a state-of-the-art review", *Steel Compos. Struct.*, **20**(1), 21-41.
- Sabbagh, A.B., Petkovic, M., Pilakoutas, K. and Mirghaderi, R. (2013), "Cyclic behaviour of bolted cold-formed steel moment connections: FE modelling including slip", *J. Constr. Steel Res.*, **80**, 100-108.
- Sabbagh, A.B., Petkovic, M., Pilakoutas, K. and Mirghaderi, R. (2012), "Experimental work on cold-formed steel elements for earthquake resilient moment frame buildings", *Eng. Struct.*, **42**,

371-386.

- Wrzesien, A.M., Lim, J.B.P., Xu, Y., MacLeod, I.A. and Lawson, R.M. (2015) "Effect of stressed skin action on the behaviour of cold-formed steel portal frames", *Eng. Struct.*, **105**, 123-136.
- Yousefi, A.M., Lim, J.B.P. and Clifton G.C. (2017a), "Cold-formed ferritic stainless steel unlipped channels with web openings subjected to web crippling under interior-two-flange loading condition-Part I: Tests and finite element model validation", *Thin Wall. Struct.*, **116**, 333-341.
- Yousefi, A.M., Lim, J.B.P. and Clifton G.C. (2017b), "Cold-formed ferritic stainless steel unlipped channels with web openings subjected to web crippling under interior-two-flange loading condition-Part II: Parametric study and design equations", *Thin Wall. Struct.*, **116**, 342-356.
- Zhang, X., Rasmussen, K.J.R. and Zhang, H. (2015), "Structural modelling of cold-formed steel portal frames", *Struct.*, **4**, 58-68.
- Zhang, X., Rasmussen, K.J.R. and Zhang, H. (2016), "Experimental investigation of locally and distortionally buckled portal frames", *J. Constr. Steel Res.*, **122**, 571-583.
- Zhou, W. and Jiang, L. (2017), "Distortional buckling of cold-formed lipped channel columns subjected to axial compression", *Steel Compos. Struct.*, **23**(3), 331-338.

BU

## Nomenclature

$a$	Length of triangular area of apex bracket
$a_B$	Length of bolt-group
$b$	Edge width of apex bracket
$b_B$	Breadth of bolt-group
$D$	Depth of web of channel-section
$d_s$	Depth of stiffener of apex bracket
$M_u$	Ultimate moment capacity
$M_u^{ana}$	$M_u$ from finite element analysis
$M_u^{exp}$	$M_u$ from test
$t$	Thickness of channel-section or bracket
$\sigma_{ult}$	Ultimate stress
$\sigma_y$	Yield stress